Cell Reports
Physical Science

CellPress

Article

Light-Driven Electrochemical Carbon Dioxide Reduction to Carbon Monoxide and Methane Using Perovskite Photovoltaics

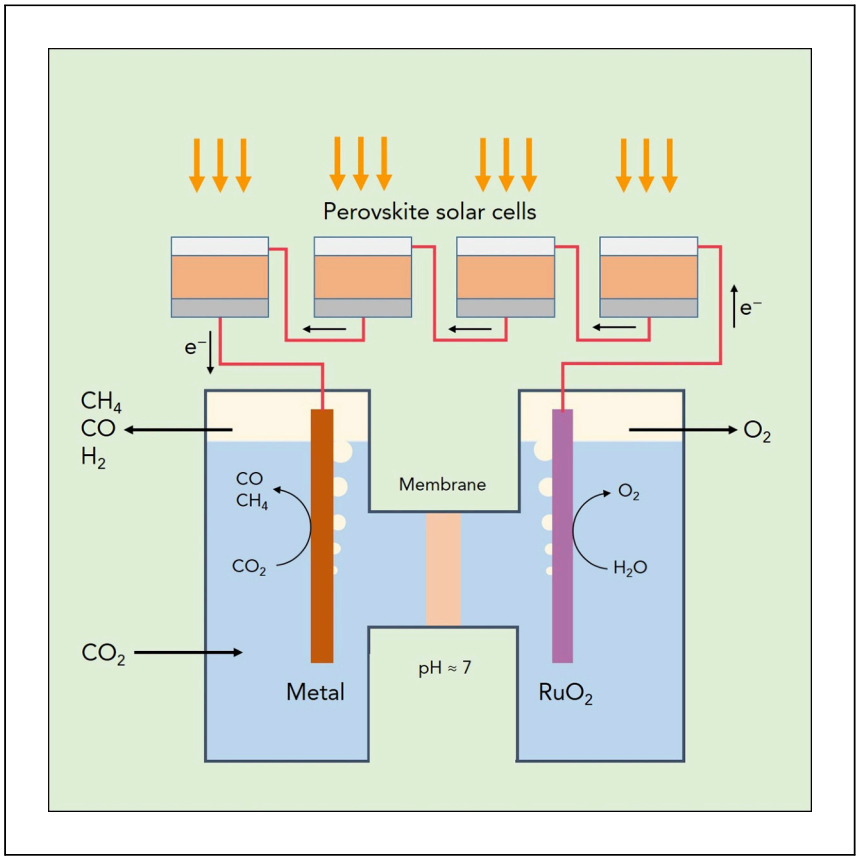

Esiner et al. demonstrate electrochemical conversion of carbon dioxide to carbon monoxide and methane using energy from sunlight. By using efficient perovskite solar cells and appropriate metal and metal oxide catalysts, they achieve light-driven conversion of carbon dioxide reduction at considerable solar-to-fuel conversion efficiencies for several hours.

Serkan Esiner, Junke Wang, René A.J. Janssen

r.a.j.janssen@tue.nl

HIGHLIGHTS

Solar-powered electrochemical carbon dioxide reduction at near neutral pH

Solar-to-carbon monoxide efficiency is >8% for 4.5 h using a gold catalyst

Solar-to-methane efficiency is close to 2% for 8 h using a copper catalyst

Increasing lifetime and activity of the copper catalyst via 1-min pauses

Esiner et al., Cell Reports Physical Science *1*, 100058
May 20, 2020
https://doi.org/10.1016/j.xcrp.2020.100058

Cell Reports
Physical Science

CellPress
OPEN ACCESS

Article

Light-Driven Electrochemical Carbon Dioxide Reduction to Carbon Monoxide and Methane Using Perovskite Photovoltaics

Serkan Esiner,[1] Junke Wang,[1] and René A.J. Janssen[1,2,3,*]

SUMMARY

Storing solar energy in chemical bonds is an effective strategy to overcome the intermittency of sunlight as an energy source. Here, we demonstrate unassisted light-driven electrochemical aqueous carbon dioxide reduction to carbon monoxide and methane using *p-i-n* double-cation lead halide perovskite solar cells in combination with catalytic electrodes for carbon dioxide reduction and water oxidation at near-neutral pH. Three series-connected photovoltaic cells and gold and ruthenium(IV) oxide electrodes provide carbon monoxide with >8% solar-to-carbon monoxide conversion efficiency for 4.5 h. Including concomitant hydrogen formation, the total solar-to-fuel conversion efficiency remains >8.3% for 10 h. Four series-connected cells with copper and ruthenium(IV) oxide electrodes provide methane. The longevity of the copper electrode improves by setting the cell to open circuit for 1 min every 15 min. The solar-to-methane conversion efficiency is close to 2%, and including 3% solar-to-hydrogen conversion efficiency, the solar-to-fuel conversion efficiency is 5% for 8 h.

INTRODUCTION

At the Earth's surface, sunlight is intermittent in time and place. To use solar energy as a renewable energy source on a large scale, it is important to develop effective storage solutions. Combining photovoltaic with electrochemical conversion to convert solar energy into energetic chemical bonds is an attractive strategy for high-density energy storage. While light-driven water splitting is attractive in terms of energy efficiency and the reversible chemical cycle of hydrogen in formation and combustion, hydrogen suffers from a low volumetric energy density. Light-driven electrochemical conversion of carbon dioxide (CO_2) to methane (CH_4), ethylene (C_2H_4), formic acid (HCOOH), or carbon monoxide (CO) not only contributes to storing renewable energy but it may also reduce increasing atmospheric CO_2 levels.

The energy required for electrochemical reduction of CO_2 depends on the target product and is further determined by catalysts, electrolyte, membrane, and dimensions of the electrochemical system. As an example, the thermodynamic potential for CO_2 reduction to CO is 1.34 V, but the complexity of the reaction, especially at the cathode side, increases the potential for the reaction to >2 V. Transition metal surfaces catalyze electrochemical CO_2 reduction by facilitating electron transfer using *d*-orbital electrons.[1,2] Hori et al.[3] extensively studied and optimized conditions for CO_2 reduction using bulk metals. The selectivity of transition metals toward various products is determined by the overpotential for the formation of reaction

[1]Molecular Materials and Nanosystems and Institute for Complex Molecular Systems, Eindhoven University of Technology, PO Box 513, 5600 MB Eindhoven, the Netherlands

[2]Dutch Institute for Fundamental Energy Research, De Zaale 20, 5612 AJ Eindhoven, the Netherlands

[3]Lead Contact

*Correspondence: r.a.j.janssen@tue.nl

https://doi.org/10.1016/j.xcrp.2020.100058

intermediates and products. These overpotentials are related to the strength of adsorption of the intermediates and products on the metal surface. Au and Ag are suitable for CO formation owing to the weak binding between CO and the metal.[1] Cu is the only transition metal with considerable activity for CH_4 formation. Metals such as Sn, In, and Pb show strong catalytic activity for reduction to formate.

Faradaic efficiencies of 90% have been achieved for the electrochemical reduction of CO_2 to CO using Au electrodes.[4] Nanostructuring of the Au surface can promote active sites and increase the surface area and thereby reduce overpotentials, enhance selectivity toward CO, and minimize material usage. Oxide-derived Au, for example, was shown to have improved stability and reduced overpotential toward CO formation due to the increased stabilization of a reaction intermediate on the gold surface.[5] Other surface structures include nanoparticles,[6] nanowires,[7] and nanoporous constructions.[8,9] Examples of non-precious metals include Cu nanoparticle electrodes prepared by electrochemical reduction of micron-thick CuO_2 films[10] and porous hollow-fiber Cu electrodes for CO production.[11]

Light-driven CO_2 reduction to CO has been demonstrated using photoelectrodes,[8,12,13] series-connected single-junction solar cells,[14–16] and multiple-junction[17,18] inorganic solar cells. A standalone solar-to-fuel device developed by Jeon et al.[16] used 5 series-connected copper indium gallium selenide (CIGS) solar cells in combination with an Earth-abundant cobalt oxide (Co_3O_4) nanoparticle catalyst for water oxidation and a nanostructured Au catalyst for CO_2 reduction to reach an overall solar-to-CO conversion efficiency of 4.23%. Higher efficiencies for CO_2 reduction to CO were reported by Schreier et al.[14] using 3 series-connected perovskite solar cells in combination with an oxidized Au electrode for CO_2 reduction and an IrO_2 anode for water oxidation. The solar-to-CO conversion efficiency was >6.5%, and including H_2 production, the total solar-to-fuel conversion efficiency exceeded 7% during an 18-h experimental frame.

CO_2 reduction requires near-neutral pH conditions. At high pH values, CO_2 is converted into carbonate and becomes unreactive, while at low pH, water reduction with H_2 evolution is predominant.[19] A bipolar membrane allows using electrolytes with different pH values on opposite sides of the membrane in an electrochemical cell, such that anolyte and catholyte can be selected independently, resulting in reduced overpotentials. Using a bipolar membrane, a solar-to-CO conversion efficiency of 13.4% has been achieved by Schreier et al.[17] The electrochemical cell uses a bifunctional Earth-abundant CuO/SnO_2 catalyst at the anode and cathode and a bipolar membrane to separate the pH 13 anolyte from the pH 6.75 catholyte. CO_2 reduction took place at 2.38 V owing to the bipolar membrane and catalyst, which reduce the overpotential. A 28.5% efficient triple-junction GaInP/GaInAs/Ge photovoltaic cell was used and the overall solar-to-fuel conversion efficiency, including H_2 and $HCOO^-$ production, was 14.4%. Furthermore, a compact electrochemical cell design and large-area electrodes (20 cm^2) and membranes (10 cm^2) contributed to reducing overpotentials and electrical resistance.

Wang et al.[20] combined solar CO_2 reduction with energy storage in a redox couple. An electrodeposited nano-gold catalyst for CO_2 reduction was coupled with a nickel-iron (NiFe) hydroxide electrode for water oxidation. The electrochemical cell consists of a bipolar membrane and 2 electrolytes with a pH difference. Next to CO_2 reduction, the electrochemical cell was designed to store energy in a zinc/zincate Zn/Zn(II) redox couple, mimicking the dark reaction in photosynthesis. When combined with a 37.9% efficient triple-junction InGaP/GaAs/Ge solar cell, a

solar-to-CO conversion efficiency of 15.6% was achieved for this system, with an average Faradaic efficiency of 92% for CO formation.

These studies have focused on maximizing solar-to-fuel conversion efficiencies, long-term stability, usage of Earth-abundant catalysts, and optimizing system parameters for light-driven electrochemical reduction of CO_2 to CO. Examples for light-driven CO_2 reduction to hydrocarbons, however, are scarce. Gurudayal et al.[21] reached >5% efficiency for conversion of sunlight into hydrocarbons and oxygenates using a stack of III–V/Si tandem solar cells in combination with a nanostructured Cu-Ag bimetallic cathode for CO_2 reduction and an IrO_2 anode for water oxidation. Huan et al.[22] have used perovskite solar cells for the conversion of CO_2 into hydrocarbons such as ethylene and ethane with a total solar-to-hydrocarbon conversion efficiency of 2.3%. A CuO-based catalyst has been used both for CO_2 reduction and water oxidation. A stack of series- and parallel-connected perovskite solar cells was combined with a continuous-flow electrochemical cell for reducing the mass transfer limitations of CO_2 and managing the resistive losses. Ren et al.[23] have reached a solar-to-ethylene conversion efficiency of 1.5% by combining oxide-derived Cu and IrO_x catalysts with a stack of silicon solar cells. A 31.9% Faradaic efficiency for ethylene formation has been reported, with a total solar-to-fuel conversion efficiency of 2.9% when liquid fuels are also included.[23]

Here, we demonstrate unassisted light-driven electrochemical CO_2 reduction to CO and to CH_4 during elongated periods of 7 to 10 h using series-connected metal halide perovskite solar cells. Perovskite solar cells have shown a remarkable improvement in performance and stability in a short period, and recently reached certified efficiencies of 25.2%.[24] Halide perovskite solar cells typically provide ~1 V at open circuit and need to be connected in series or stacked in a multiple-junction configuration for light-driven CO_2 reduction. Using perovskite solar cells, we achieve solar-to-CO energy efficiencies up to 8.9%, with Faradaic efficiencies above 80% for CO production for 7 h. Including the H_2 production, the total solar-to-fuel conversion efficiency is 8.3%–9.0% for 10 h. We also present stable CH_4 production for 8 h, with a Faradaic efficiency close to 40% using a Cu electrode. To increase the lifetime of the Cu electrode against catalyst deactivation, we apply a non-energy-consumption regeneration step every 15 min. When combined with perovskite solar cells, we demonstrate a solar-to-CH_4 conversion efficiency close to 2% for >8 h. When H_2 production is also considered, the total solar-to-fuel conversion efficiency stays at 5% through the experimental frame.

RESULTS

Light-Driven Electrochemical Reduction of CO_2 to CO

For light-driven electrochemical CO_2 reduction to CO, planar *p-i-n* metal halide perovskite solar cells were used. The cells use poly[bis(4-phenyl)(2,4,6-trimethylphenyl)amine (PTAA) as the hole transport layer and [6,6]-phenyl-C_{61}-butyric acid methyl ester (PCBM) as the electron transport layer, which sandwich a double-cation perovskite $FA_{0.66}MA_{0.34}PbI_{2.85}Br_{0.15}$ (FA is formamidinium, MA is methylammonium) photoactive layer. The single-junction solar cells have a power conversion efficiency (η_{PV}) of 17.4% and provide an open-circuit voltage (V_{oc}) of 1.02 V, a short-circuit current density (J_{sc}) of 21.0 mA cm^{-2}, and a fill factor (FF) of 0.81 under illumination with simulated AM1.5G (100 mW cm^{-2}) light. The external quantum efficiencies (EQEs) of 4 nominally identical perovskite solar cells are shown in Figure S1 and reveal negligible differences.

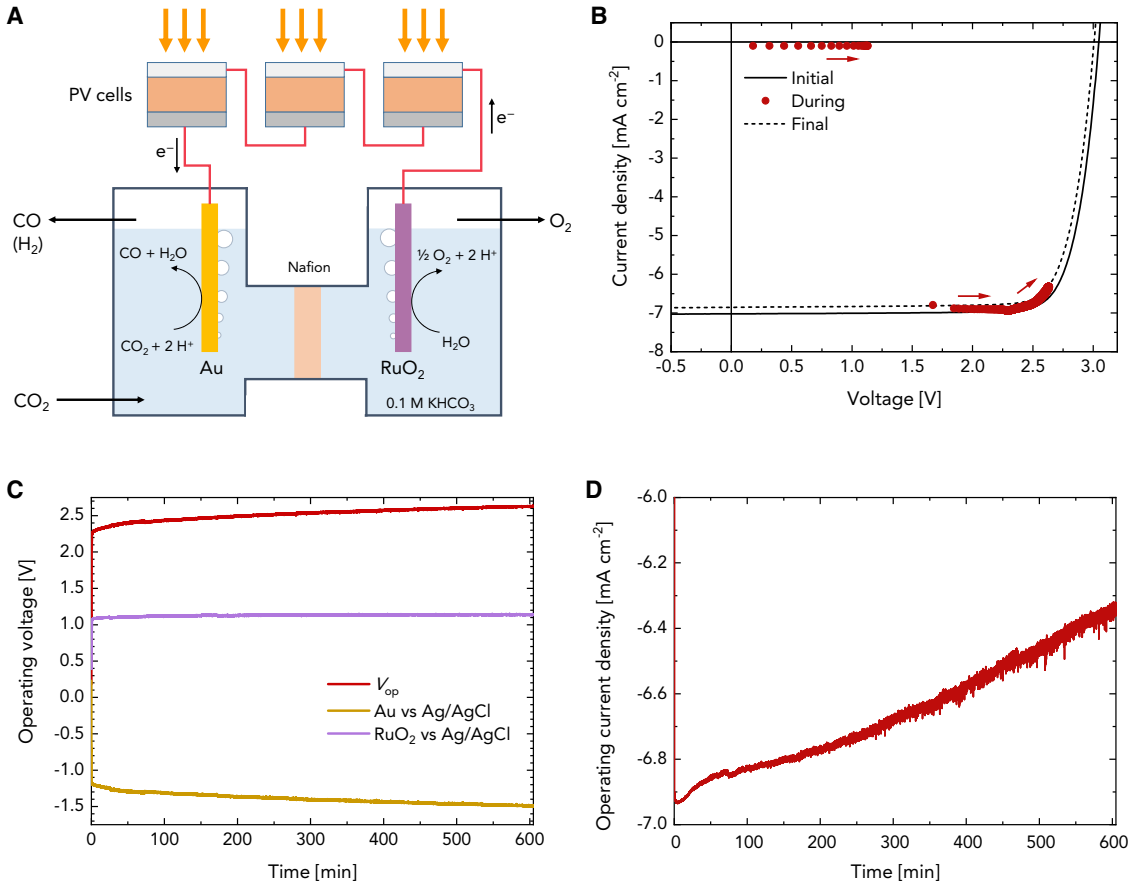

Figure 1. Light-Driven Electrochemical Reduction of CO_2 to CO

(A) Schematic of the light-driven electrochemical device for reduction of CO_2 to CO.

(B) *J-V* characteristics of 3 series-connected perovskite solar cells before, during, and after 600-min light-driven CO_2 reduction. Markers represent V_{op}, J_{op} combinations during operation, and the arrows indicate the evolution with time.

(C) V_{op}, potential difference between the Au electrode and an Ag/AgCl reference electrode, and the difference between these 2 versus time.

(D) J_{op} versus time.

Light-driven electrochemical conversion experiments were performed in an H cell (Figure 1A). An Au wire was used as the cathode for reducing CO_2 to CO. The anode for water oxidation was an RuO_2 catalyst deposited on a Ti substrate. The compartments were separated by a Nafion membrane. CO_2 reduction reaction requires a pH-neutral environment. We used 0.1 M $KHCO_3$ as a catholyte, with a pH of ~7.4, which decreased to 6.8 after CO_2 saturation. A 0.1 M $KHCO_3$ solution was also used as an anolyte. This balances the ion concentration on both sides of the membrane, reducing osmosis, but at the cost of an increased cell potential compared to using 2 different electrolytes.

The cathode product selectivity depends on the potential applied to the Au electrode.[11,16] At low potentials, a considerable proportion of H_2 forms. At intermediate potentials, CO formation increases and then peaks, due to an increasing formation of H_2 at higher overpotentials. Therefore, it is crucial to establish the potential window and current density for the cathode to operate. An Au electrode with a surface area of 0.3 cm^2 operates optimally in the selected electrolyte and for the current provided by the solar cells. On the water oxidation side, an RuO_2 catalyst with a geometric surface area of ~3 cm^2 was used on a Ti substrate. Under these conditions, the

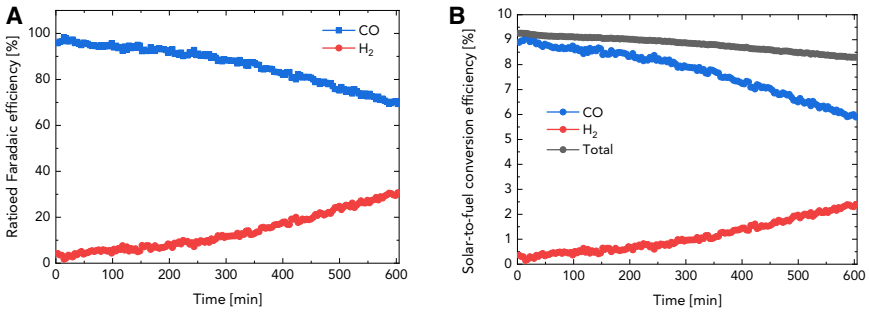

Figure 2. Efficiencies of the Light-Driven Electrochemical Reduction of CO_2 to CO

(A) Fractions of CO and H_2 generated versus time.

(B) Solar-to-fuel conversion efficiencies for CO and H_2 formation versus time.

electrochemical process requires a cell potential of ~2.5 V for efficient CO_2 reduction to CO. Optimal performance in electrochemical CO_2 reduction driven by a solar cell requires a good match of current and voltage characteristics of the 2 systems. For minimal energy loss, the maximum power point of the photovoltaic cells should be close to the operating potential (V_{op}) of the electrochemical cell. More specifically, the desired electrochemical conversion should have a high Faradaic efficiency at the maximum power voltage (V_{max}) of the solar cell. To provide the 2.50 V required for electrochemical CO_2 reduction to CO, 3 single-junction solar cells were connected in series. The resulting 3-cell module has an efficiency of 17.4% with V_{oc} = 3.05 V, J_{sc} = 7.0 mA cm^{-2}, and FF = 0.81. The maximum power point of the 3-cell module (V_{max} = 2.66 V) matches well with the operating voltage requirement of the electrochemical cell (V_{op} = 2.5 V). After masking the 3 cells to an area of 0.0314 cm^2 each, they provide a photocurrent in the range of 0.5–0.7 mA in solar light.

The electrochemical cell was connected to 3 series-connected perovskite solar cells for unassisted light-driven conversion of CO_2 to CO (Figure 1A). The solar cells were illuminated with simulated AM1.5G light and the current and voltage characteristics were monitored for 600 min of continuous operation. During this measurement, the operating voltage and current density (J_{op}) were measured together with the potential difference between the Au electrode and an Ag/AgCl reference electrode. The solar cells show stable performance with a slight reduction in V_{oc} and J_{sc} of the 3-cell module after 600 min of continuous illumination (Figure 1B). The markers show the time trajectory of the operating point (V_{op}, J_{op}) of the combined photovoltaic and electrochemical conversion. Figure 1C shows the evolution of the operating cell potential and the potential difference between the Au electrode and an Ag/AgCl reference electrode versus time. Initially, the system operates at ~2.2 V, but V_{op} gradually increases to 2.7 V over the course of 600 min as a consequence of the deactivation of the Au surface during the CO_2 reduction. The deactivation is caused by impurities in the electrolyte and coverage of the active sites on the Au surface with carbon or other intermediates. These make the electrode less active for CO formation and increase H_2 formation.[29] Figure 1C shows that the potential at the RuO_2 electrode is very stable during the experiment. The operating current density (J_{op}) reduces over the course of the experiment, following the solar cell *J-V* characteristics (Figure 1D). This is mainly due to the increased overpotential for CO_2 reduction on the cathode.

Figure 2A shows the fractions of CO and H_2 generated during 600 min as determined from the Faradaic efficiencies (see Supplemental Experimental Procedures). The

selectivity for CO is initially very high, >90%. The CO fraction remains >80% during the first 400 min and reaches 70% at 600 min. A reason for the increased H_2 production may be poisoning of the active sites on the Au electrode for CO formation. In such a case, the system moves to a regime in which the operating voltage is increased and H_2 generation is enhanced.

The amounts of CO and H_2 formed and the solar cell efficiency determine the overall solar-to-fuel conversion efficiency. Figure 2B shows that the solar-to-CO conversion efficiency is 8.9% at the start of the 600-min experiment. The efficiency remains >8% for 280 min and is among the highest solar-to-CO conversion efficiencies found using perovskite solar cells.[14,25] After 280 min, the solar-to-CO conversion efficiency reduces at a higher rate, reaching 5.9% after 600 min. This decrease is compensated for by an increase in the formation of H_2. At 600 min, 2.5% solar-to-H_2 conversion efficiency is reached. Considering the combined CO and H_2 formation, the total solar-to-fuel conversion efficiency starts at >9% and ends at 8.3% after 600 min. The continuous decrease in total solar-to-fuel conversion efficiency is in part due to the differences in the energy contents between CO and H_2 and in part caused by the decreasing operating current (J_{op}; Figure 1D) during the experiment as a consequence of the deactivation of the Au electrode and the perovskite solar cells.

Because a higher electrolyte concentration can reduce resistive losses and increase the efficiency, we checked the effect of raising the bicarbonate concentration from 0.1 M to 1 M $KHCO_3$. Figure S2 shows that a 1-M $KHCO_3$ concentration results in a decrease in selectivity for CO formation from 90% to 55%, although the stability increased. The enhanced H_2 formation, increasing from 10% to 45%, is attributed to the higher H^+ concentration near the cathode.[26]

Light-Driven Electrochemical Reduction of CO_2 to CH_4

For the reduction of CO_2 to CH_4, we selected Cu as catalyst, which is known to give the highest CH_4 production rate when used as a bulk metal compared to other transition metals.[3,27] As mentioned above, the overpotentials depend on the desired end product and the electrodes used. Since the focus is to produce hydrocarbons instead of CO, the dynamics on the cathode side are inevitably different. Hydrocarbons such as CH_4 and C_2H_4 go through different reaction pathways and require the transfer of many more electrons than does CO formation. Consequently, higher overpotentials occur in the formation and desorption of intermediates and products. In our experiments, we observed that CH_4 production typically occurs at more negative potentials of $\sim$−1.7 V versus Ag/AgCl, compared to $\sim$−1.3 V for CO production.[3] Combined with water oxidation, a total cell voltage of $\sim$3 V is required. When designing the electrochemical cell, a balance between the high voltage requirement and low current is necessary. At low voltages, CH_4 cannot be formed; however, when the voltage is too high, the increased current introduces high resistive losses in the cell. For appropriate balancing, we have optimized the electrochemical cell using a current of 2 mA. The size of the Cu electrode and the solar cell area have been tuned with respect to this current.

The electrochemical cell used for hydrocarbon production is similar to the H cell used for CO production but uses a Cu wire (0.2 cm^2) as a cathode instead of Au. As a catholyte, various salts and concentrations were tested. Optimal results were obtained using 0.25 M $NaHCO_3$.[19,28] To balance the ionic strength on both sides of the membrane, 0.25 M $NaHCO_3$ was also used as an anolyte. A Nafion membrane

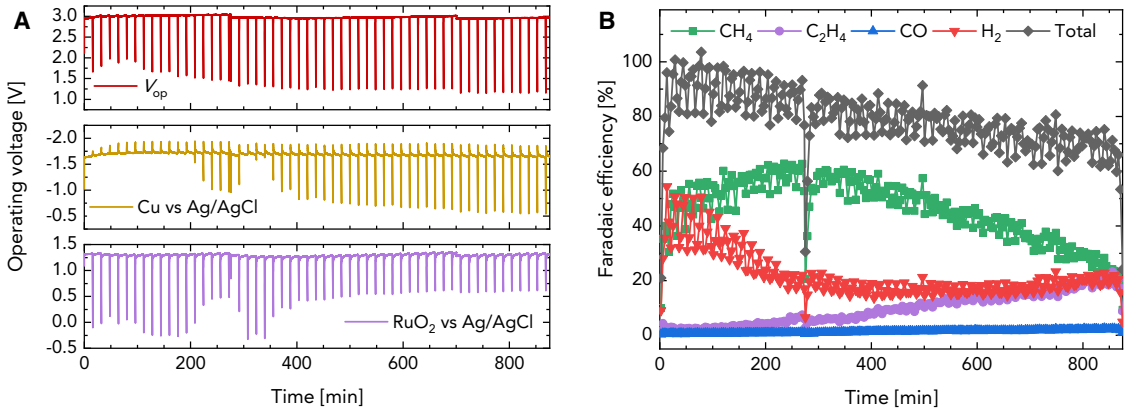

Figure 3. Electrochemical Reduction of CO_2 to CH_4

(A) Total cell potential, potential difference between the Cu electrode and an Ag/AgCl reference electrode, and difference between these 2 versus time. During intervals of 15 min, 2 mA was applied, followed by 1 min at 0.09 V to regenerate the Cu cathode.

(B) Faradaic efficiencies of the generated products versus time.

was used between the compartments, and the anode was RuO_2 (3 cm^2) on a Ti substrate.

To understand and optimize hydrocarbon formation at the Cu electrode, several experiments using this electrochemical cell were performed. The initial experiments resulted in very fast deactivation of the Cu electrode, resulting in the exclusive production of H_2 after 1 to 2 h of operation. In most of these experiments, the surface of the Cu electrode turned black. This deactivation of the Cu electrode has been frequently addressed in the literature. Metal impurities in the electrolyte have been pointed at as a reason, and a pre-electrolysis procedure has been suggested to reduce this effect.[29] X-ray photoelectron spectroscopy (XPS) analysis on a Cu electrode indicates that the electrode surface is covered with graphitic carbon,[30] possibly formed from formate.[31] Various attempts focused on eliminating this effect or on elongating the lifetime of the Cu electrode by applying pulsed instead of continuous potentials for CO_2 reduction,[32,33] or by anodizing the Cu electrode.[34] We found that the deactivation of the Cu electrode can be largely reversed by applying a near-zero potential to the electrochemical cell. Figure 3A shows the evolution of V_{op} when sourcing a constant current of 2 mA to the electrochemical cell for CO_2 to CH_4 reduction. After 15 min, when the Cu surface starts becoming darker, the source-measurement unit (SMU) was set at a potential of 0.09 V for 1 min. Since the open-circuit potential of the electrochemical cell is ~0.9 V, the cell goes into reverse operation at a potential of 0.09 V, resulting in the oxidation of the dark coverage on the Cu electrode, which becomes clean and regains its metallic luster. This effect not only elongates the lifetime of the electrode but it also increases the performance during the first 4 h, as can be seen in Figure 3B. The apparent scatter in the Faradaic efficiency curves is due to the 1-min breaks, which result in the dilution of the remaining products with the continuous CO_2 inlet flow. The 15-min cycles clearly appear, and the most reliable data points are the ones at the end of the cycles, which correspond to the maxima.

When continued for >800 min, this method significantly increases the lifetime of the Cu catalyst for the production of hydrocarbons. Despite the improvement, the Faradaic efficiency for CH_4 reduces from a maximum value of 60% after 250 min to 20% at 800 min. This loss is in part compensated for by C_2H_4 formation, which starts increasing after ~350 min, and reaches a Faradaic efficiency of 20% at the end.

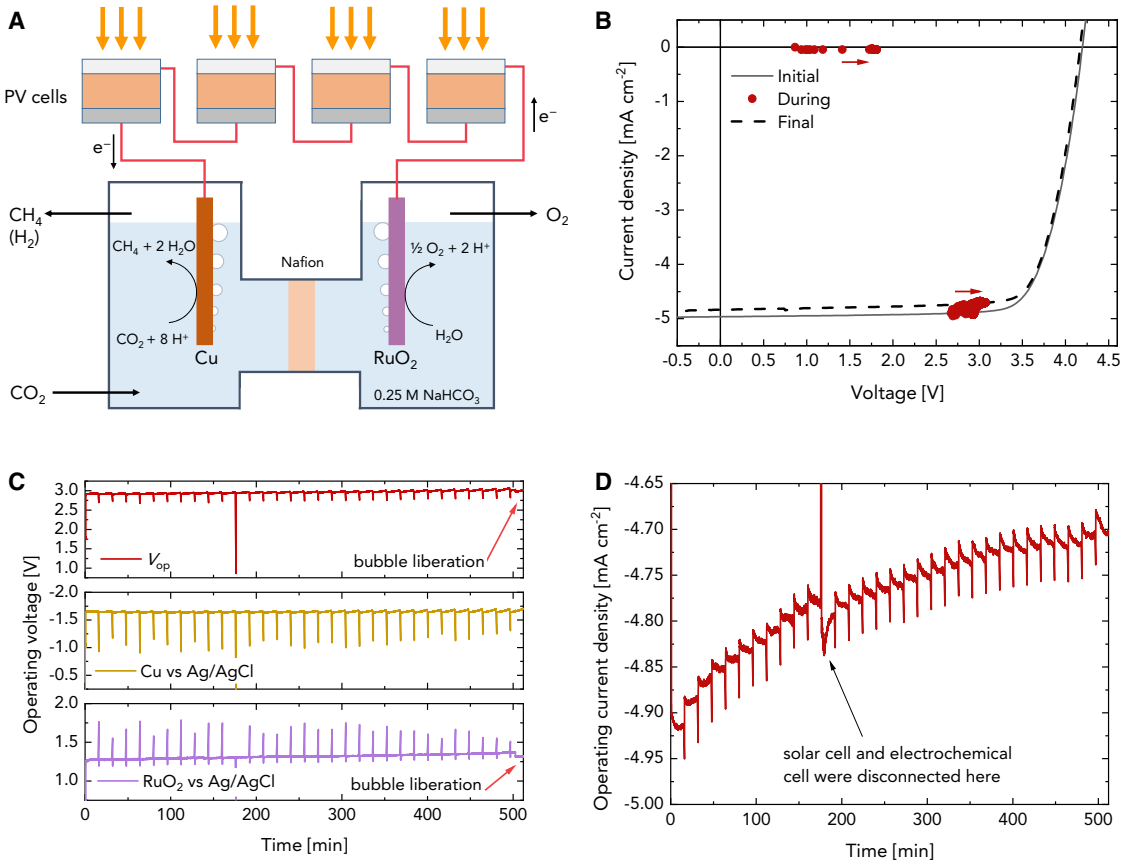

Figure 4. Light-Driven Electrochemical Reduction of CO_2 to CH_4

(A) Schematic of the light-driven electrochemical device for reduction of CO_2 to CH_4.

(B) *J-V* characteristics of 4 series-connected perovskite solar cells before, during, and after 510-min light-driven CO_2 reduction. Markers represent V_{op}, J_{op} combinations during operation, and the arrows indicate the evolution with time.

(C) V_{op}, potential difference between the Cu electrode and an Ag/AgCl reference electrode, and the difference between these 2 versus time. Every 15 min, the electrical connection between the solar cells and the electrochemical cell was interrupted by switching the SMU to a high-impedance off-mode to regenerate the Cu electrode. In this off-mode, no voltage or current values were recorded. The physical disconnection at $t = 176$ min took place in the on-mode, where the current and voltage data points were recorded.

(D) J_{op} versus time.

Although helpful, it is also clear that this method does not provide a thorough solution for the deactivation problem, and at the end of the experiment, the Cu electrode is visually deactivated by a dark coverage.

A V_{op} of ~3 V is required to run the selected electrochemical cell for CH_4 formation (Figure 3A). This implies that 4 single-junction perovskite ($FA_{0.66}MA_{0.34}PbI_{2.85}Br_{0.15}$) solar cells must be connected in series (Figure 4A). To provide sufficient current, cell areas of 0.0936 cm^2 per single-junction cell were used. The power conversion efficiency of such solar cells is η_{PV} = 16.5%, with J_{sc} = 20.7 mA cm^{-2}, V_{oc} = 1.05 V, and FF = 0.76. In a 4-cell module, the resulting power conversion efficiency was η_{PV} = 16.2%, with J_{sc} = 4.96 mA cm^{-2}, V_{oc} = 4.20 V, and FF = 0.78 (Figure 4B). The maximum power voltage is V_{max} = 3.45 V and well above the V_{op} = 3 V operating point of the electrochemical cell. This results in some additional loss in the energy conversion when the electrochemical cell is combined with the 4-cell module, but it gives the system enough room for stabilization during any unstable operation and increase of overpotentials.

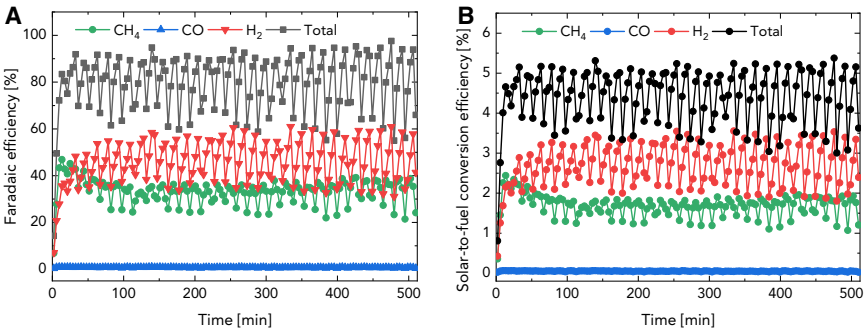

Figure 5. Efficiencies of the Light-Driven Electrochemical Reduction of CO_2 to CH_4

(A) Faradaic efficiencies of CH_4, CO, and H_2 generated versus time.

(B) Solar-to-fuel conversion efficiencies for CH_4, CO, and H_2 formation versus time.

For the purpose of light-driven CO_2 reduction to CH_4, the stack of 4 series-connected perovskite cells was electrically coupled to the electrochemical cell (Figure 4A). The solar cell was illuminated continuously with simulated AM1.5G light for 510 min. Figure 4B shows the solar cell characteristics before and after the experiment. The solar cell showed a stable performance, with only a slight reduction in current generation after 510 min. To mimic the regeneration step of the Cu electrode, the 4-cell solar module and the electrochemical cell were disconnected for 1 min after every 15 min. This brings the electrochemical cell to open circuit, which is less effective in regenerating the Cu electrode than bringing it to an oxidation potential state when using the SMU because no current can flow. Remarkably, a regeneration effect is still observed. Apparently, the potential drop on the Cu electrode during the 1-min break induces the products deposited to be desorbed from the Cu surface, reactivating the Cu electrode electrochemically and visibly.

The top panel in Figure 4C shows the operating potential of the cells during the 510-min experimental time span. The center panel in Figure 4C shows the potential difference between the Cu electrode and an Ag/AgCl reference electrode. The potential on the RuO_2 electrode together with the resistive losses (bottom panel in Figure 4C) were determined by subtracting the potential on the Cu electrode from the total cell potential. The operating point of the system and the potential on the Cu electrode were very stable during the 510-min experiment. The minor increase in the overall cell potential (~0.09 V between 50 and 500 min) was mainly due to the accumulation of bubbles next to the Nafion membrane that reduce the membrane surface area and increase the resistive losses. Manually liberating a bubble next to the membrane at the 500th min immediately reduced the overall cell potential by 0.06 V, resulting in a net increase of only 0.03 V over 450 min. Figure 4D shows a continuous but slight reduction in J_{op}. This reduction is mainly due to the slight increase in the overall cell potential combined with a slight degradation of the solar cell. This shifts the operating point along the *J-V* curve of the 4-cell module.

Figure 5A shows the Faradaic efficiency for CH_4, H_2 and CO formation during the 510-min light-driven electrochemical reduction. The CH_4 formation remains very stable at ~40% Faradaic efficiency for 510 min, and H_2 production stabilizes at ~60%. Hence, the trends in CH_4 and H_2 formation are somewhat different from that shown in Figure 3B. Unlike the experiment in which the electrochemical cell is set to 0.09 V during the 1-min breaks, no increase in CH_4 formation was observed in the first 250 min when disconnecting the electrochemical cell. No

C_2H_4 formation was observed. A constant trace amount of CO production was detected. After 8 h, the Cu electrode was still visibly very shiny, which is a sign of negligible deactivation.

The Faradaic efficiencies were combined with the efficiencies of the 4-cell module to estimate the overall solar-to-fuel conversion efficiency. The time-average solar-to-CH_4 conversion efficiency is estimated to be ~2% (Figure 5B). Together with a solar-to-H_2 conversion efficiency of ~3%, an overall solar-to-fuel conversion efficiency of 5% is reached. When taking the 1-min interruption every 15 min into account, the CH_4 and H_2 yields decrease by ~0.1 and 0.2 percentage points, respectively. Even though solar-to-CH_4 conversion efficiency is at low levels, it is a very stable 8-h experiment, and to our knowledge the first demonstration of light-driven CO_2 reduction to CH_4 with perovskite solar cells.

Figures S3 and S4 show that with continuous operation (i.e., without the 15 min on followed by 1 min off method), a Cu electrode affords an initial Faradaic efficiency for CH_4 of ~60%, which decreases to 20% after 180 min and to 10% after 360 min. The Cu electrode becomes darker, and a continuous increase in H_2 formation is observed up to a Faradaic efficiency of almost 60%. The potential difference between the Cu electrode and the Ag/AgCl reference electrode also decreases due to a lower overpotential for H_2 production compared to CH_4 production. As a consequence, the solar-to-fuel conversion efficiency of ~5% is similar to the experiment with the 15 + 1-min method, but the solar-to-CH_4 conversion efficiency is only ~0.5% after 360 min.

Critical Analysis and Outlook

Unassisted light-driven electrochemical CO_2 reduction on a large scale poses a complex engineering problem. Optimal performance requires balancing the area of the photovoltaic panels with those of the electrodes and catalysts. In the present study, solar cell-cathode-anode geometric area ratios of ~1:3:30 for CO production and of ~2:1:15 for CH_4 were used that are feasible in laboratory experiments, but not in practice. For electrodes, micro- and nanostructuring or porosity can increase the effective surface area compared to the geometric area and reduce the current densities compared to those provided by the solar cells. Some of these limitations can also be alleviated by the use of a gas diffusion electrode (GDE), in which CO_2 reduction to CO can effectively take place at high current densities, due to reduced mass transport limitations with an increased contact period between CO_2 and the catalyst.[35] Consequently, limitations due to CO_2 solubility in aqueous electrolytes are reduced.[36] Improvements in the cell design, such as the use of a flow cell, can increase the overall performance of the electrochemical cell by altering the conditions in the cell such as diffusion and local pH.[35,37] Flow cell configurations can also contribute to minimizing the distance between the 2 electrodes, resulting in reduced resistance losses. In the H cell configuration, the system must be operated in a certain potential range to maintain a high selectivity for CO. However, CO_2 reduction in a flow cell with GDE can allow for a large range of current densities in which CO selectivity is high.[38] Thus, the electrochemical cell is less sensitive to changes in the operating current density and hence to variations in solar irradiance.

DISCUSSION

We have demonstrated unassisted light-driven CO_2 reduction to CO and CH_4 using perovskite solar cells. With an Au cathode and RuO_2 anode for H_2O oxidation, CO formation takes place at ~2.5 V at near-neutral pH with a Faradaic efficiency

>80% for 7 h. Solar-to-CO conversion efficiency maximized at 8.9% and was >8% for 4.5 h. Including the concomitant H_2 formation, the total solar-to-fuel conversion efficiency remains >8.3% for 10 h. A similar light-driven electrochemical configuration, using a Cu cathode, was used for CO_2 to CH_4 reduction. A 15-min on/1-min off method significantly increased the catalytic lifetime of the Cu electrode applied during 8 h. Stable CH_4 formation with a Faradaic efficiency of almost 40% was achieved for 8 h. The electrochemical cell operated at ~3 V. A stable solar-to-CH_4 conversion efficiency close to 2% was achieved over the full course of the experiment. The reaction also afforded a constant solar-to-H_2 conversion efficiency of ~3%, which, together with the CH_4 formation, results in a total of 5% solar-to-fuel conversion efficiency.

When the energetic losses are considered, a major loss still occurs in the photovoltaic conversion. However, the electrochemical conversion efficiencies are also far from unity. For CO production, these are close to 50% and for CH_4 formation <15%. The losses are mainly due to the differences in the thermodynamic potential (E_0) and the operating voltage (V_{op}) required to perform the catalytic reactions. The E_0:V_{op} ratio for CO is ~0.54 and for CH_4 ~0.35. In addition, for CH_4 the Faradaic efficiency is only ~40% and V_{op} = 3 V is less than V_{max} = 3.45 V for the 4-cell module. New catalysts that reduce the overpotentials for CO and CH_4 formation, and simultaneously increase the overpotential for H_2 formation, are required to reduce these losses. Next to the development of novel catalysts, the design of the electrochemical conversion system can be improved to reduce resistance losses in the cell. A larger membrane surface area and smaller electrode distance will reduce resistive losses. Further improvements can be achieved by controlling the impurities in the system and possibly the temperature. For CH_4 production, it has been shown that the Faradaic efficiency increases with decreasing reaction temperature.[27,39] Such future developments will increase the significant solar-to-fuel conversion efficiencies reached here and enable efficient and stable direct light-driven conversion of CO_2 into fuels.

EXPERIMENTAL PROCEDURES

Resource Availability

Lead Contact

Further information and requests for resources should be directed to and will be fulfilled by the Lead Contact, René Janssen (r.a.j.janssen@tue.nl).

Materials Availability

This study did not generate new unique reagents.

Data and Code Availability

The authors declare that data supporting the findings of this study are available within the paper and the Supplemental Information. All other data are available from the Lead Contact upon reasonable request.

Materials

PTAA (M_w = 14.5 kg mol^{-1}) was obtained from EM Index and PCBM (99%) was obtained from Solenne BV. PbI_2 (99.99% trace metal basis) was purchased from TCI Chemicals. Formamidinium iodide (FAI), methylammonium iodide (MAI), and methylammonium bromide (MABr) were obtained from Greatcell Solar. *N*,*N*-Dimethylformamide (DMF, anhydrous 99.8%) dimethyl sulfoxide (DMSO, anhydrous 99.9%), chlorobenzene (CB, anhydrous 99.8%), 2-propanol, chloroform (CF), and toluene were obtained from Sigma-Aldrich.

Au wire used as the electrode for CO production had a diameter of 1 mm and a purity of 99.9999%. Cu wire was obtained from Alfa Aesar and had a diameter of 0.5 mm and a purity of 99.9999%. Ruthenium(III) chloride (35%–40% Ru) used for RuO_2 catalyst preparation was obtained from Acros Organics. All electrolytes and aqueous solutions were prepared using water that is purified in a Millipore system and that has a resistivity of at least 18 MΩ cm. $KHCO_3$ used in the electrolytes was obtained from Acros Organics and had a purity of ≥99.7%. $NaHCO_3$ used in the electrolytes had EMSURE ACS, Reag. Ph Eur (reagent part of the European Pharmacopoeia) grade purity and was obtained from Merck. Phosphoric acid, 85%, for etching the Cu wire was obtained from Sigma-Aldrich. CO_2 used in the experiments had a 4.0 grade purity and was obtained from the Linde Group. The calibration gases used for the gas chromatograph were obtained from the Linde Group in 1-l ECOCYL cylinders. One calibration gas consisted of 5 ppm methane, ethane, ethylene, carbon monoxide, and hydrogen in a nitrogen balance. A second had the same contents at 100-ppm concentration per gas.

A custom-made gas-tight H cell was used for the electrochemical CO_2 reduction experiments. Connections between the cell and the gas chromatograph were made with 1/8-inch perfluoroalkoxy (PFA) tubing and Swagelok connections. The Nafion-115 membrane used in the electrochemical cell was obtained from Alfa Aesar and had a thickness of 0.125 mm. An Ag/AgCl Aldrich glass reference electrode was used during 3-electrode measurements. The electrode was treated with 3 M KCl solution.

Solar Cell Fabrication

Pre-patterned glass/InSnO (ITO) substrates (Naranjo) were cleaned by sonication in acetone, soapy water (sodium dodecyl sulfate, Acros, 99%), deionized water, and 2-propanol, respectively. Before use, the substrates were cleaned under UV ozone for 30 min. PTAA was dissolved in toluene at a concentration of 3 mg mL^{-1} and stirred at 60°C. PbI_2 (553 mg) was dissolved in DMF (0.876 mL) and DMSO (87.6 μL) at 60°C. FAI (54.0 mg), MAI (14.3 mg), and MABr (7.6 mg) were dissolved in 2-propanol (1 mL) at 60°C. PCBM (20 mg) was dissolved in a 1:1 CB:CF solvent mixture (1 mL) and stirred at room temperature. The PTAA solution was spin coated in an N_2 glovebox onto the ITO substrates at 5,700 rpm (20,000 rpm/s acceleration) for 30 s and annealed at 100°C for 10 min. After cooling, the perovskite layer was deposited using a sequential deposition method. The PbI_2 solution was spin coated at 3,000 rpm (2,000 rpm/s acceleration) for 30 s, followed by the spin coating of the FAI/MAI/MABr solution at 3,300 rpm for 30 s. The substrate was immediately annealed at 100°C for 30 min. Afterward, the PCBM solution was spin coated on the perovskite film at 1,000 rpm (20,000 rpm/s acceleration) for 60 s and annealed at 100°C for 30 min. The sample was then transferred to a thermal evaporator, where LiF (1 nm) and Al (100 nm) were sequentially deposited under a high vacuum (~3×10^{-7} mbar). The overlap of the top Al electrode and the bottom ITO contact determines the active area of the solar cell.

RuO_2 Catalysts from Thermal Decomposition

RuO_2 catalysts were deposited on Ti substrates with a thickness of 0.5 mm and a geometrical surface area of 1.5 cm × 2.0 cm. The Ti substrates were first sonicated in acetone and then treated with air plasma for 2 min at 270 W before the deposition of the catalyst. A Femto low-pressure plasma system from Diener Electronics was used for the plasma treatment. The RuO_2 catalysts were prepared by first dissolving 0.2 M $RuCl_3$ in purified water. A total of 200 μL of this solution was then placed on the Ti substrate. This substrate was first dried for 20 min on a 90°C hot plate. The

oxidation then took place in a 350°C oven for 3 h. The resulting geometrical RuO_2 area per substrate was ~1.5 cm^2. During electrochemical CO_2 reduction experiments, 2 of these substrates were clamped together back to back, resulting in a total area of ~3 cm^2.

Electrode Preparation

The Cu wire was cleaned by mechanical polishing with sandpaper, followed by electropolishing. The electropolishing process was adopted from the literature and is performed in 85% phosphoric acid, applying 4.0 V anodic potential for 5 min, with respect to a Ti electrode.[10,26] A Cu surface area of ~0.2 cm^2 is in contact with the electrolyte during experiments. Au electrodes were prepared by mechanical polishing with sandpaper, followed by sonication in purified water for 15 min. An Au surface area of ~0.3 cm^2 is in contact with the electrolyte during experiments.

Electrochemical Measurements

A 3-compartment gas-tight cell was used during measurements, in which the compartments for working and counter electrodes are separated with a Nafion-115 membrane with a surface area of 3.14 cm^2. The 2 electrodes were 6.5 cm apart and the membrane was positioned at equal distances from both electrodes. The compartment with the reference cell was connected to the working electrode compartment with a Luggin capillary. Both anode and cathode electrolytes were stirred at 400 rpm during the measurements. The cathode compartment was saturated with a continuous CO_2 flow of 30 mL min^{-1}, controlled by an EL-FLOW Prestige mass flow controller obtained from Bronkhorst Nederland. The catholyte was saturated with CO_2 before the experiments.

The gaseous products were analyzed online, using a 3-channel gas analyzer. This compact gas chromatograph (CGC 4.0) was obtained from Global Analyzer Solutions-Interscience B.V. and was controlled by Chromeleon 7 software (Thermo Fisher Scientific). During the CO_2 reduction process, the CO_2 leaves the cathode compartment of the electrochemical cell, and together with the products, continuously circulates through the gas chromatograph. Once in every 3.8 min, a sample is taken into the gas chromatograph for analysis. A flame ionization detector (FID) detector is tuned to measure methane, ethylene, and ethane contents. A second FID detector with a methanizer is tuned to measure the CO content and a thermal conductivity detector (TCD) measures the H_2 content inside the samples received from the electrochemical cell. The gas chromatograph is calibrated at 2 points using calibration bottles with 5 and 100 ppm of methane, ethane, ethylene, carbon monoxide, and hydrogen contents in a nitrogen balance. The electrolytes were not analyzed to detect formate and other products that are dissolved in the electrolyte. Further details on determining the Faradaic efficiency can be found in the Supplemental Experimental Procedures and Figure S5.

Characterization

The current density to voltage (*J-V*) characteristics of the solar cells were measured under ~100 mW cm^{-2} white light illumination from a tungsten-halogen lamp, filtered by a Schott GG385 UV filter and a Hoya LB120 daylight filter. No mismatch correction was performed. The measurements were performed using a Keithley 2400 source-measurement unit. The solar cells were kept inside a glove box with a nitrogen atmosphere during characterization. Short circuit currents were calculated more accurately by the integration of EQE with the AM1.5G solar radiation.

For single-junction cells, during the fast *J-V* scan, the voltage was swept either from +1.5 to −0.5 V (reverse scan) or from −0.5 to +1.5 V (forward scan) at a scan rate of 0.25 V s^{-1}. For stabilized *J-V* measurements, the solar cell was kept at open circuit for 5 min under light soaking, followed by a reverse sweep from (V_{oc} + 0.04) V to −0.04 V, with a step size of 0.04 V; the acquisition time of current density at each voltage step was 5 s. The voltage at the maximum power point was determined from the stabilized *J-V* curve.

EQE measurement was performed in a nitrogen atmosphere. The probe light source was generated by a 50-W tungsten-halogen lamp (Philips FocusLine), which was modulated with a mechanical chopper (Stanford Research, SR 540) before passing into a monochromator (Oriel, Cornerstone 130). The spectral response of the device was recorded as a voltage from a pre-amplifier (Stanford Research, SR 570) using a lock-in amplifier (Stanford Research, SR 830), and was calibrated by a reference silicon cell. To accurately determine the current density, a green light-emitting diode (LED) (530 nm, Thorlabs M530L3, driven by a DC4104 driver) was used as a light bias to provide the solar cell with ∼1 sun illumination intensity during the measurement.

The light-driven CO_2 reduction experiments were performed using a home-built solar simulator with ∼100 mW cm^{-2} white light illumination from a tungsten-halogen lamp, filtered by a Schott GG385 UV filter and a Hoya LB120 daylight filter. Since the electrochemical CO_2 reduction experiments took place in air, the solar cells were kept behind a quartz window in a nitrogen-filled box and connected to the catalysts through external cabling. Each substrate included 4 solar cells. For CO formation, 3 of these cells were connected in series, each having a restricted surface area of 0.0314 cm^2, giving a total cell area of 0.0942 cm^2. For CH_4 formation, 4 of these cells were connected in series, each having a restricted surface area of 0.0936 cm^2, giving a total cell area of 0.3744 cm^2. The solar cells were positioned carefully to match the short circuit current values under AM1.5G standards. Keithley 2400 and 2600 SMUs were used for simultaneous measurement of current and voltages during the light-driven electrochemical CO_2 reduction processes. The SMUs were controlled by Autolab scripts. A Keithley 2400 was used for measuring the voltage on the working electrode (Au or Cu) with respect to the Ag/AgCl reference electrode. A 2-channel Keithley 2600 was used to measure the current flow and the total voltage between the anode and the cathode during the CO_2 reduction process. The measurements with 1-min breaks were also controlled through Autolab scripts by setting the current-measuring channel of the SMU to high-impedance "off-mode." This then breaks the circuit between the solar cell and the electrochemical cell, putting the electrochemical cell into the open circuit conditions of ∼0.9 V, which allows for partial recovery of the catalyst deactivation process. In the electrochemical experiments (Figure 3), the Cu electrode was regenerated by setting the cell potential to 0.09 V for 1 min with the SMU.

Faradaic efficiencies were determined by first determining the theoretical rate of generation. This requires knowledge of the current (*I* in A) flowing through the electrochemical cell, the CO_2 volumetric flow rate (*Q* in L min^{-1}), and the number of electron transfers (*n*) required to produce the specific product. The theoretical rate (*R*) for generation of a specific product is then $R = 60I/nF$[mol min^{-1}], where *F* is the Faraday constant. Assuming an ideal gas at room temperature and 1 bar, 1 mol gaseous product corresponds to 24.5 L, and the theoretical concentration in the exit flow is $C_{th} = (1470I/nFQ) \times 10^6$ ppm. The Faradaic efficiency of that product is then determined by taking the ratio of its concentration (*C* in parts per million)

measured by the gas chromatograph with C_{th}: $FE = (C/C_{th}) \times 100\%$. In these calculations, n = 2 for CO, n = 2 for H_2, n = 8 for CH_4, and n = 12 for C_2H_4.

The solar-to-fuel energy conversion efficiency ($\eta_{S\text{-}to\text{-}F}$) is determined by taking the ratio of the input energy from the sunlight to the energy content of the generated product. This efficiency can also be split into the product of photovoltaic conversion efficiency (η_{PV}) and electrochemical conversion efficiency (η_{EC}), via $\eta_{S-to-F} = \eta_{PV} \cdot \eta_{EC}$. The photovoltaic conversion efficiency is the ratio of the output power density of the solar cell during operation ($P_{out} = J_{op} V_{op}$, where V_{op} and J_{op} are the voltage and current density of the solar cell during operation) with the input power density (P_{in} = 100 mW cm^{-2}): $\eta_{PV} = (J_{op}V_{op}/P_{in}) \times 100\%$. The electrochemical conversion efficiency is the ratio of the thermodynamic potential for the formation of a specific product (E_0) and the potential at which the electrochemical reaction takes place (V_{op}), multiplied by the Faradaic efficiency (FE):$\eta_{EC} = (E_0/V_{op})FE \times 100\%$. When put together, the solar-to-fuel efficiency is given by $\eta_{S-to-F} = (E_0 J_{op}/P_{in})FE \times 100\%$. The E_0 values used are 1.34 V for CO, 1.23 V for H_2, 1.06 V for CH_4, and 1.15 V for C_2H_4.

SUPPLEMENTAL INFORMATION

Supplemental Information can be found online at https://doi.org/10.1016/j.xcrp.2020.100058.

ACKNOWLEDGMENTS

We thank Dr. Matthew Dyson, Mr. Joost van Dongen, Mr. David van Impelen, Dr. Koen Hendriks, and Dr. Martijn Wienk for their technical assistance and helpful discussions. The research was funded by the Interreg Flanders-Netherlands program Project EnOp, the Ministry of Education, Culture, and Science (Gravity program 024.001.035), and the NWO Spinoza prize awarded to R.A.J. Janssen by the Netherlands Organization for Scientific Research (NWO).

AUTHOR CONTRIBUTIONS

S.E. and R.A.J.J. conceived and designed the research. S.E. performed the electrochemical and light-driven electrochemical experiments and device characterization. J.W. fabricated the perovskite solar cells. S.E. and R.A.J.J. wrote the manuscript, with help from J.W.

DECLARATION OF INTERESTS

The authors declare no competing interests.

Received: February 11, 2020
Revised: March 23, 2020
Accepted: April 3, 2020
Published: May 20, 2020

REFERENCES

1. Kuhl, K.P., Hatsukade, T., Cave, E.R., Abram, D.N., Kibsgaard, J., and Jaramillo, T.F. (2014). Electrocatalytic conversion of carbon dioxide to methane and methanol on transition metal surfaces. J. Am. Chem. Soc. *136*, 14107–14113.

2. Hori, Y., Wakebe, H., Tsukamoto, T., and Koga, O. (1994). Electrocatalytic process of CO selectivity in electrochemical reduction of CO_2 at metal electrodes in aqueous media. Electrochim. Acta *39*, 1833–1839.

3. Hori, Y., Kikuchi, K., and Suzuki, S. (1985). Production of CO and CH_4 in electrochemical reduction of CO_2 at metal electrodes in aqueous hydrogencarbonate solution. Chem. Lett. *14*, 1695–1698.

4. Hori, Y., Murata, A., Kikuchi, K., and Suzuki, S. (1987). Electrochemical reduction of carbon dioxide to carbon monoxide at a gold electrode in aqueous potassium hydrogen carbonate. J. Chem. Soc. Chem. Commun. 728–729.

5. Chen, Y., Li, C.W., and Kanan, M.W. (2012). Aqueous CO_2 reduction at very low

overpotential on oxide-derived Au nanoparticles. J. Am. Chem. Soc. *134*, 19969–19972.

6. Zhu, W., Michalsky, R., Metin, Ö., Lv, H., Guo, S., Wright, C.J., Sun, X., Peterson, A.A., and Sun, S. (2013). Monodisperse Au nanoparticles for selective electrocatalytic reduction of CO_2 to CO. J. Am. Chem. Soc. *135*, 16833–16836.

7. Zhu, W., Zhang, Y.-J., Zhang, H., Lv, H., Li, Q., Michalsky, R., Peterson, A.A., and Sun, S. (2014). Active and selective conversion of CO_2 to CO on ultrathin Au nanowires. J. Am. Chem. Soc. *136*, 16132–16135.

8. Song, J.T., Ryoo, H., Cho, M., Kim, J., Kim, J.-G., Chung, S.-Y., and Oh, J. (2017). Nanoporous Au thin films on Si photoelectrodes for selective and efficient photoelectrochemical CO_2 reduction. Adv. Energy Mater. *7*, 1601103.

9. Lu, Q., Rosen, J., Zhou, Y., Hutchings, G.S., Kimmel, Y.C., Chen, J.G., and Jiao, F. (2014). A selective and efficient electrocatalyst for carbon dioxide reduction. Nat. Commun. *5*, 3242.

10. Li, C.W., and Kanan, M.W. (2012). CO_2 reduction at low overpotential on Cu electrodes resulting from the reduction of thick Cu_2O films. J. Am. Chem. Soc. *134*, 7231–7234.

11. Kas, R., Hummadi, K.K., Kortlever, R., de Wit, P., Milbrat, A., Luiten-Olieman, M.W.J., Benes, N.E., Koper, M.T.M., and Mul, G. (2016). Three-dimensional porous hollow fibre copper electrodes for efficient and high-rate electrochemical carbon dioxide reduction. Nat. Commun. *7*, 10748.

12. Andrei, V., Reuillard, B., and Reisner, E. (2020). Bias-free solar syngas production by integrating a molecular cobalt catalyst with perovskite-$BiVO_4$ tandems. Nat. Mater. *19*, 189–194.

13. Jang, Y.J., Jeong, I., Lee, J., Lee, J., Ko, M.J., and Lee, J.S. (2016). Unbiased sunlight-driven artificial photosynthesis of carbon monoxide from CO_2 using a ZnTe-based photocathode and a perovskite solar cell in tandem. ACS Nano *10*, 6980–6987.

14. Schreier, M., Curvat, L., Giordano, F., Steier, L., Abate, A., Zakeeruddin, S.M., Luo, J., Mayer, M.T., and Grätzel, M. (2015). Efficient photosynthesis of carbon monoxide from CO_2 using perovskite photovoltaics. Nat. Commun. *6*, 7326.

15. Urbain, F., Tang, P., Carretero, N.M., Andreu, T., Gerling, L.G., Voz, C., Arbiol, J., and Morante, J.R. (2017). A prototype reactor for highly selective solar-driven CO_2 reduction to synthesis gas using nanosized earth-abundant catalysts and silicon photovoltaics. Energy Environ. Sci. *10*, 2256–2266.

16. Jeon, H.S., Koh, J.H., Park, S.J., Jee, M.S., Ko, D.-H., Hwang, Y.J., and Min, B.K. (2015). A monolithic and standalone solar-fuel device having comparable efficiency to photosynthesis in nature. J. Mater. Chem. A Mater. Energy Sustain. *3*, 5835–5842.

17. Schreier, M., Héroguel, F., Steier, L., Ahmad, S., Luterbacher, J.S., Mayer, M.T., Luo, J., and Grätzel, M. (2017). Solar conversion of CO_2 to CO using Earth-abundant electrocatalysts prepared by atomic layer modification of CuO. Nat. Energy *2*, 17087.

18. Sugano, Y., Ono, A., Kitagawa, R., Tamura, J., Yamagiwa, M., Kudo, Y., Tsutsumi, E., and Mikoshiba, S. (2015). Crucial role of sustainable liquid junction potential for solar-to-carbon monoxide conversion by a photovoltaic photoelectrochemical system. RSC Advances *5*, 54246–54252.

19. Hori, Y. (2008). Electrochemical CO2 reduction on metal electrodes. In Modern Aspects of Electrochemistry, *Vol. 42*, C.G. Vayenas, R.E. White, and M.E. Gamboa-Aldeco, eds. Modern Aspects of Electrochemistry (Springer), pp. 89–189.

20. Wang, Y., Liu, J., Wang, Y., Wang, Y., and Zheng, G. (2018). Efficient solar-driven electrocatalytic CO_2 reduction in a redox-medium-assisted system. Nat. Commun. *9*, 5003.

21. Gurudayal, Bullock, J., Srankó, D.F., Towle, C.M., Lum, Y., Hettick, M., Scott, M.C., Javey, A., and Ager, J. (2017). Efficient solar-driven electrochemical CO_2 reduction to hydrocarbons and oxygenates. Energy Environ. Sci. *10*, 2222–2230.

22. Huan, T.N., Dalla Corte, D.A., Lamaison, S., Karapinar, D., Lutz, L., Menguy, N., Foldyna, M., Turren-Cruz, S.-H., Hagfeldt, A., Bella, F., et al. (2019). Low-cost high-efficiency system for solar-driven conversion of CO_2 to hydrocarbons. Proc. Natl. Acad. Sci. USA *116*, 9735–9740.

23. Ren, D., Loo, N.W.X., Gong, L., and Yeo, B.S. (2017). Continuous production of ethylene from carbon dioxide and water using intermittent sunlight. ACS Sustain. Chem. Eng. *5*, 9191–9199.

24. National Renewable Energy Laboratory (2020). Best Research-Cell Efficiencies. https://www.nrel.gov/pv/assets/pdfs/best-research-cell-efficiencies.20200128.pdf.

25. Chen, J., Dong, C., Idriss, H., Mohammed, O.F., and Bakr, O.M. (2020). Metal halide perovskites for solar-to-chemical fuel conversion. Adv. Energy Mater. *10*, 1902433.

26. Hori, Y., Murata, A., and Takahashi, R. (1989). Formation of hydrocarbons in the electrochemical reduction of carbon dioxide at a copper electrode in aqueous solution. J. Chem. Soc., Faraday Trans. I *85*, 2309–2326.

27. Hori, Y., Kikuchi, K., Murata, A., and Suzuki, S. (1986). Production of methane and ethylene in electrochemical reduction of carbon dioxide at copper electrode in aqueous hydrogencarbonate solution. Chem. Lett. *15*, 897–898.

28. Kyriacou, G.Z., and Anagnostopoulos, A.K. (1993). Influence of CO_2 partial pressure and the supporting electrolyte cation on the product distribution in CO_2 electroreduction. J. Appl. Electrochem. *23*, 483–486.

29. Hori, Y., Konishi, H., Fautamura, T., Murata, A., Koga, O., Sakurai, H., and Oguma, K. (2005). "Deactivation of copper electrode" in electrochemical reduction of CO_2. Electrochim. Acta *50*, 5354–5369.

30. DeWulf, D.W., Jin, T., and Bard, A.J. (1989). Electrochemical and surface studies of carbon dioxide reduction to methane and ethylene at copper electrodes in aqueous solutions. J. Electrochem. Soc. *136*, 1686–1691.

31. Wasmus, S., Cattaneo, E., and Vielstisch, W. (1990). Reduction of carbon dioxide to methane and ethene—an on-line MS study with rotating electrodes. Electrochim. Acta *35*, 771–775.

32. Shiratsuchi, R., Aikoh, Y., and Nogami, G. (1993). Pulsed electroreduction of CO_2 on copper electrodes. J. Electrochem. Soc. *140*, 3479–3482.

33. Engelbrecht, A., Uhling, C., Stark, O., Hämmerle, M., Schmid, G., Magori, E., Wiesner-Fleischer, K., Fleischer, M., and Moos, R. (2018). On the electrochemical CO_2 reduction at copper sheet electrodes with enhanced long-term stability by pulsed electrolysis. J. Electrochem. Soc. *165*, J3059–J3068.

34. Jermann, B., and Augustynski, J. (1994). Long-term activation of the copper cathode in the course of CO_2 reduction. Electrochim. Acta *39*, 1891–1896.

35. Weekes, D.M., Salvatore, D.A., Reyes, A., Huang, A., and Berlinguette, C.P. (2018). Electrolytic CO_2 reduction in a flow cell. Acc. Chem. Res. *51*, 910–918.

36. De Luna, P., Hahn, C., Higgins, D., Jaffer, S.A., Jaramillo, T.F., and Sargent, E.H. (2019). What would it take for renewably powered electrosynthesis to displace petrochemical processes? Science *364*, 350.

37. Endrődi, B., Bencsik, G., Darvas, F., Jones, R., Rajeshwar, K., and Janáky, C. (2017). Continuous-flow electroreduction of carbon dioxide. Progr. Energy Combust. Sci. *62*, 133–154.

38. Salvatore, D.A., Weekes, D.M., He, J., Dettelbach, K.E., Li, Y.C., Mallouk, T.E., and Berlinguette, C.P. (2018). Electrolysis of gaseous CO_2 to CO in a flow cell with a bipolar membrane. ACS Energy Lett. *3*, 149–154.

39. Kaneco, S., Hiei, N.-h., Xing, Y., Katsumata, H., Ohnishi, H., Suzuki, T., and Ohta, K. (2002). Electrochemical conversion of carbon dioxide to methane in aqueous $NaHCO_3$ solution at less than 273 K. Electrochim. Acta *48*, 51–55.